RSC Advances

ROYAL SOCIETY OF CHEMISTRY

www.rsc.org/advances

Graphical Abstract

Self-assembled platinum compounds resulting in stable, highly emissive and long-lived species are reported for cell imaging.

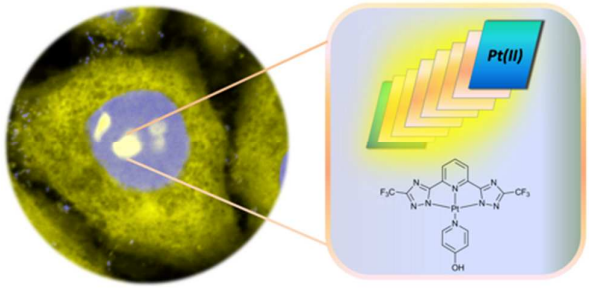

Journal Name

RSCPublishing

ARTICLE

Bio-imaging with neutral luminescent Pt(II) complexes showing metal···metal interactions†

Cite this: DOI: 10.1039/x0xx00000x

Dedy Septiadi,[a] Alessandro Aliprandi,[a] Matteo Mauro,*[,a,b] and Luisa De Cola*[,a]

Received 00th January 2012,
Accepted 00th January 2012

DOI: 10.1039/x0xx00000x

www.rsc.org/

Molecular bio-imaging based on optical detection is facing important challenges in the attempt to develop new materials and small molecules able to have better emission quantum yield, stability toward photobleaching and long excited-state lifetime. A strategy to achieve these properties is to use triplet emitters based on metal complexes and protect them from dioxygen quenching. We report on an interesting approach based on the use of self-assembled platinum compounds in order to obtain stable, highly emissive and long-lived species. Cell internalization and localization experiments show that the assemblies possess a different selectivity towards cellular compartments dictated by the terdentate ligand coordinated to the platinum. Also, the conditions used for the incubation determine cell internalization of the platinum complexes or their expulsion in the media.

1. Introduction

In the past decades organometallic compounds containing transition metals have attracted much attention for both fundamental and applied research. The combination of metal ions and ligands for the formation of metal complexes leads to a series of properties, which are unique in terms of reactivity, photochemistry, photophysics and redox. In particular, transition metal complexes, TMCs, based on first row, *e.g.* Cu(I), second and third row with d^6 electronic configuration, such as Ir(III), Ru(II) and Re(I), d^8 *e.g.* Pt(II), d^{10} *e.g.* Au(I), are amongst the most investigated systems. Their photochemical and thermal stability, wide modulation of the emission colour,[1-2] high photoluminescence quantum yield (PLQY) with values up to unity,[3-4] good solution- and/or vacuum-processability and the possibility to electrically populate the luminescent excited states, make them good candidates for solid-state light-emitting devices and optoelectronics application.[5-12]

Another major research field in which luminescent TMCs are currently attracting great deal of attention is their use for sensing of bio-related molecules,[13-17] and as luminescent labels for bio-imaging[18-22]. Even though fluorescent organic and bio-organic labels are still the leading choice for such applications mostly due to their excitation and emission tunability,[23-25] the use of phosphorescent TMCs is taking over because of the enormous advantages that the latters might show over the formers.[18-22]

In this respect, apart from the wide emission colour tunability above mentioned, most luminescent TMCs are *i*) more stable towards photo- and chemical degradation; *ii*) they display a very large Stokes shift that allows the detection of their emission at a much lower energy than the excitation energy; *iii*) their lowest-lying luminescent excited state is triplet in nature and therefore they possess long-lived excited states. Also, many of the investigated complexes possess excited states of charge transfer nature thus making them sensitive to the environment in terms of polarity and rigidity, while long-lived luminescence allows dioxygen detection. In bio-medical applications this last property is of particular importance since an improvement of the signal over background auto-fluorescence[26-27] ratio, by means of time-gated techniques, can be achieved.[28] However, to maintain high emission quantum yield and long excited state lifetime in water and in particular in the presence of dioxygen is a big challenge. In fact, a bimolecular quenching of the emission is in general observed and its efficiency is related to the excited state lifetime and the amount of molecular oxygen dissolved in the environment. To prevent the decrease of the emission intensity, a strategy followed by several authors is the encapsulation of the emitters in the core of dendrimers[29-32] or other large shielding structures such as vesicles and micelles to limit the diffusion of the quencher.[33] The combination of the sensitivity towards the environment and the large range of excited state lifetimes (from nano- to micro-seconds), has been successfully used for time-resolved imaging techniques such as fluorescence and

phosphorescence lifetime imaging mapping, namely FLIM and PLIM, respectively.[34]

Another limitation of the luminescent TMCs *vs* organic dyes is their low absorption in the visible region. Indeed, their excitation is typically achieved by using UV light, which has a very limited penetration into tissues and causes damage of biological specimens due to the high-energy content. These severe drawbacks hamper the successful employment of luminescent TMCs for imaging in living cells, in tissue and *in vivo*. Developing systems that can be excited and emit in the red to NIR in order to minimize auto-fluorescence as well as tissue light absorption and scattering is highly desirable and a challenge.[26-27,35-37]

Amongst all luminescent TMCs, platinum(II) complexes play a leading role in several applications because of their great photophysical properties and interesting structural characteristics. In particular, the high tendency towards stacking through π–π and closed-shell metallophilic interactions facilitated by their square-planar geometry is appealing for the protection of the metal complex from the environment. Noteworthy, such $d^8\cdots d^8$ interaction, which typically shows distances in the range 3–3.5 Å, leads to lower-lying excited state with metal-metal-to-ligand charge transfer (MMLCT) character and in some cases enhancement of the emission properties.[38-40]

Herein, we report on how the use of neutral square-planar platinum(II) complexes, consisting of a terdentate ligand containing a pyridine bis-triazole coordinating moiety, could be a successful strategy towards the development for high luminescent and long-lived imaging probes. We also demonstrate how upon establishment of metallophilic interactions, formation of the MMLCT band can be advantageously used for inducing a sizeable bathochromic shift of both excitation and emission while enhancing PLQY. Finally, the formation of such aggregates results in reduced photobleaching of the probes and in a sizeable prolongation of their excited-state lifetime in living human cervical carcinoma, HeLa, cells incubated with the here reported platinum derivatives.

2. Experimental Section

2.1 Material and methods

All the reactions were carried out under nitrogen atmosphere. All the solvents and reagents were used as received from Aldrich, Fluka, TCI and VWR without further purification. K_2PtCl_4 was purchased from Precious Metal Online (PMO). $PtCl_2(DMSO)_2$,[41] and 2,6-*bis*(3-(*p*-tolyl)-1*H*-1,2,4-triazol-5-yl)pyridine (**py-Tol-trzH_2**)[42] were prepared by following already reported synthetic procedures. All the synthesis and characterization of the ligands and the complexes are described below. Column chromatography was performed on silica gel 60 (particle size 63–200 μm, 230–400 mesh, Merck). High-resolution electron spray ionization mass spectrometry (HR-ESI-MS) was performed on a Bruker Daltonics (Bremen, Germany) MicroToF with loop injection. ^{1}H and ^{19}F NMR analyses were carried out on a Bruker AMX 400 Avance. The full characterization for all the compounds is given in the ESI (see Figs S1-S4).

2.2 Syntheses of the ligands

Pyridine-2,6-biscarboxamidine dihydrochloride. 2,6-dicarbonitrile (20.0 g, 154.9 mmol, 1.0 eq.) and MeONa (1.67 g, 30.98 mmol, 0.2 eq.) were dissolved in 180 mL of dry methanol. After refluxing for 6 h, ammonium chloride (12.8 g, 340.8 mmol, 2.2 eq.) was added to the reaction mixture and kept overnight under reflux. After cooling, the solid was filtered over a Buchner, washed with Et_2O, dried and collected as pure compound (30.6 g, 130.2 mmol, yield 84.0%) ^{1}H NMR (D_2O, ppm) δ: 8.43 (m). HR-ESI-MS (*m/z*): $[M–2HCl+H]^+$ calcd. 164.0933; found 164.0931.

2,6-*bis*(3-(trifluoromethyl)-1*H*-1,2,4-triazol-5-yl)pyridine (py-CF_3-trzH_2). Ethyltrifluoroacetate (13.7 mL, 114.4 mmol, 2.2 eq.) was dissolved in 150 mL of THF and hydrazine monohydrate (6.15 mL, 126.7 mmol, 2.2 eq.) was added. The reaction mixture was refluxed for 2 h, followed by the addition of pyridine-2,6-biscarboxamidine dihydrochloride (15.0 g, 63.5 mmol, 1 eq.) and sodium hydroxide (2.54 g, 63.5 mmol, 1 eq.). The reaction mixture was kept overnight refluxing under nitrogen. After cooling, the desired product, **py-CF_3-trzH_2**, was purified from the crude on column chromatography by using silica gel as stationary phase and dichloromethane and acetone 9:1 as eluent (2.04 g, 5.84 mmol, yield 9.2%). ^{1}H NMR (CD_2Cl_2, ppm) δ: 13.82 (2H), 8.21 (2H), 8.06 (1H); ^{19}F{^{1}H} NMR (CD_2Cl_2, ppm) δ: –65.61 (1F). HR-ESI-MS (*m/z*): $[M+Na]^+$ calcd. 372.0395; found 372.0403.

2.3 Synthesis of the complexes

CF_3-Pt-4OHpy. Ligand **py-CF_3-trzH_2** (230.0 mg, 0.660 mmol, 1.0 eq.), $PtCl_2(DMSO)_2$ (306.0 mg, 0.73 mmol, 1.1 eq.), 4-hydroxypyridine (63 mg, 0.660 mmol, 1.0 eq.) and 200 μL of Et_3N were suspended in 20 mL of a 3:1 2-methoxyethanol and water. The reaction mixture was heated overnight at 85°C. A yellowish-green precipitate appeared few minutes after the heating. The desired compound was purified on column chromatography using silica gel as stationary phase and 3:1 THF:*n*-hexane mixture as eluent, and obtained as greenish-yellow solid (66.1 mg, 0.104 mmol, yield 15.7%). ^{1}H NMR (THF-d_8, ppm) δ: 9.31 (2H), 8.14 (1H), 8.72 (2H), 6.95 (2H); ^{19}F{^{1}H} NMR (THF-d_8, ppm) δ: –65.10 (1F). HR-ESI-MS(-) (*m/z*): $[M-H]^-$ calcd. 636.03246; found 636.03002.

Tol-Pt-4OHpy. The platinum(II) complex was prepared in similar condition to the above described **CF_3-Pt-4OHpy**, by employing 2,6-*bis*(3-(*p*-tolyl)-1*H*-1,2,4-triazol-5-yl)pyridine as tridentate ligand. The complex was purified on column chromatography using silica gel as stationary phase and ethylacetate:ethanol 1:1 as eluent, and obtained as yellow solid

(yield 7%). ^{1}H NMR (DMSO-d_6, ppm) δ: 9.10 (2H), 8.17 (1H), 8.01 (4H), 7.80 (2H), 7.29 (4H), 6.50 (2H), 2.36 (6H); HR-ESI-MS (*m/z*): $[M+H]^+$ calcd. 682.16388; found 682.16471.

2.4 Crystallography

X-Ray diffraction data collection was carried out on a Nonius Kappa-CCD diffractometer equipped with an Oxford Cryosystem liquid N_2 device, using Mo Kα radiation (λ = 0.71073 Å). The crystal-detector distance was 36 mm. The cell parameters were determined (Denzo software)[43] from reflections taken from one set of 10 frames (1.0° steps in phi angle), each at 20 s exposure. The structures were solved by direct methods using the program SHELXS-97.[44] The refinement and all further calculations were carried out using SHELXL-97.[45] The hydrogen atoms were included in calculated positions and treated as riding atoms using SHELXL default parameters. The non-H atoms were refined anisotropically, using weighted full-matrix least-squares on F^2. A semi-empirical absorption correction was applied using MULscanABS in PLATON.[46] Transmission factors: T_{min}/T_{max} = 0.35078/0.42889. The fluorines of one trifluoromethyl group are disordered over two positions. The structure was treated as a racemic twin solved within the P1 space group with a BASF of 0.26804. CCDC-988918 contains the crystallographic data for **CF_3-Pt-4OHpy**·2DMSO complex. These data can be obtained free of charge from the Cambridge Crystallographic Data Centre.

2.5 Photophysical measurements

All solvents used for spectroscopical characterization were spectrometric grade and purchased by VWR. Absorption spectra were measured on a Shimadzu UV-3600 spectrophotometer double-beam UV–VIS–NIR spectrometer and baseline corrected. Steady-state emission spectra were recorded on a Horiba Jobin−Yvon IBH FL-322 Fluorolog 3 spectrometer equipped with a 450 W xenon arc lamp, double-grating excitation, and emission monochromators (2.1 nm mm^{-1} of dispersion; 1200 grooves mm^{-1}) and a TBX-04 single photon-counting detector. Emission and excitation spectra were corrected for source intensity (lamp and grating) and emission spectral response (detector and grating) by standard correction curves. Time-resolved measurements were performed using the time-correlated single-photon-counting (TCSPC) option on the Fluorolog 3. NanoLEDs (402 nm; fwhm <200 ps) with repetition rates between 10 kHz and 1 MHz was used to excite the sample. The excitation sources were mounted directly on the sample chamber at 90° to a double-grating emission monochromator (2.1 nm mm^{-1} of dispersion; 1200 grooves mm^{-1}) and collected by a TBX-04 single-photon-counting detector. The photons collected at the detector are correlated by a time-to-amplitude converter to the excitation pulse. Signals were collected using an IBH DataStation Hub photon-counting module and data analysis was performed using the commercially available DAS6 software (Horiba Jobin-Yvon IBH). The quality of the fit was assessed by minimizing the reduced χ2 function and by visual inspection of the weighted residuals. For multi-exponential decays, the intensity, namely I*(t)*, has been assumed to decay as the sum of individual single exponential decays as by the following equation:

$$I(t) = \sum_{i=1}^{n} a_i e^{-\frac{t}{\tau_i}}$$

where τ_i are the decay times and a_i are the amplitude of the component at t = 0. The percentages to the pre-exponential factors, a_i, are listed upon normalization. The quantum yield measurements were performed by using an absolute photoluminescence quantum yield spectrometer Quantaurus C11347 (Hamamatsu, Japan) exciting the sample at λ_{exc} = 300 and 350 nm. All solvents were spectrometric grade. The measurements were performed on samples at 50 μM concentration.

2.6 Cell culture

All materials for cell culture were purchased from Gibco. HeLa cells were cultured inside media which contains 88% Dulbecco's Modified Eagle Medium (DMEM), 10% Fetal Bovine Serum (FBS), 1% Penicillin-Streptomycin and 1 % L-Glutamine 200 mM under 37°C and 5% of CO_2 condition for 48 hours until reaching 70 to 80% cell confluency. Subsequently, the cells were washed twice with Phosphate Buffer Solution (PBS, Gibco), trypsinated and approximately 50,000 cells were reseeded on the monolayer glass cover slip inside six-well plate culture dish and glass bottom dishes (MatTek). Fresh culture media (2 mL) was added gently and cells were overnight grown.

2.7 Platinum complexes incubation

Incubation with PBS. The culture media was removed and 2 mL of new staining solution containing the corresponding platinum complex (50 μM in less than 1% DMSO containing PBS) were gently added onto cells. After incubation at 37°C for 4 hours, the incubating media was removed and the cell layer on glass cover slips was gently washed (3×) with PBS and fixed with 4% paraformaldehyde (PFA) solution for 10 min.
Incubation with cell culture media. The culture media was removed and 50 μM of **CF_3-Pt-4OHpy** staining solution (in less than 1% DMSO containing culture media) was added to the cells grown onto glass bottom dishes. After incubation at 37°C for either 4 or 24 hours, the media was removed and the cell layer on glass cover slips was gently washed (3×) with PBS and 2 mL of fresh culture media was added.

2.8 Organelle staining

Cell layer was washed twice with PBS and kept in 0.1% Triton X-100 in PBS for 10 minutes and afterwards in 1% bovine serum albumin, BSA (Sigma Aldrich), in PBS for 20 min. The

cell layer on glass cover slip was stained with Phalloidin Alexa Fluor® 568 (Invitrogen), for F-actin/membrane staining, for 20 min, in the dark at room temperature, and washed twice with PBS. For nucleoli staining purpose, 500 nM of SYTO® RNASelect™ Green Fluorescent Cell Stain (Invitrogen) solution were added on the top of cells for 20 minutes followed by PBS washing. For visualizing nuclear region, cell nucleus was stained with 4',6-diamidino-2-phenylindole carboxamidine (DAPI) and washed twice with PBS. The cover slips were mounted onto glass slides for microscopy measurements.

2.9 Photobleaching experiments

Photobleaching experiments were carried on fixed cells priorly stained with **CF_3-Pt-4OHpy** and DAPI. The sample was continuously excited with high power 405 nm laser (32 mW) for 5 minutes and subsequently imaged at low power acquisition (1.2 mW) every 5 minutes for a total time of 25 minutes.

2.10 Kinetic of internalization of the complex in culture media

The culture media of live cells grown onto glass bottom dish was removed and 2 mL of **CF_3-Pt-4OHpy** staining solution (50 μM in less than 1% DMSO containing culture media) was added. The cells were subsequently imaged by confocal microscopy setup for one minute acquisition time for a total duration of 75 minutes.

2.11 Kinetic of cellular expulsion of the complex after culture media addition

Cells grown on glass bottom dish were incubated with 2 mL of **CF_3-Pt-4OHpy** staining solution (50 μM in less than 1% DMSO containing PBS) for 20 minutes. Subsequently, cells were quickly washed three times with PBS to eliminate the excess of the complex and PBS media was replaced by normal culture media. Confocal microscopy experiments were directly performed for 2 minutes acquisition time for a total duration of 40 minutes.

2.12 Fluorescence confocal microscopy

All of the fluorescence images were taken by using Zeiss LSM 710 confocal microscope system with 63× magnification, numerical aperture, NA, 1.3 of Zeiss LCI Plan-NEOFLUAR water immersion objective lens (Zeiss GmbH). The samples were excited by continuous wave (cw) laser at 405 nm. The emission of the complexes was collected in the range from 500 to 620 nm. In addition, the lambda-mode acquisition technique was performed to observe the emission spectra of the two complexes after cell internalization. In this case, the complexes were excited at 405 nm and emission spectra were collected from 412 to 723 nm. For co-localization experiments, the samples priorly co-stained with different dyes, DAPI (excitation/emission wavelength: 358 nm/461 nm), SYTO® RNASelect™ Green Fluorescent Cell Stain (excitation/emission wavelength: 490 nm/530 nm) and Alexa Fluor® 568 Phalloidin (excitation/emission wavelength: 578nm/600 nm) were excited at 405 nm and 594 nm, respectively. The emission spectra of the complexes together with the different dyes employed were also collected by using lambda-mode acquisition of the confocal setup. The raw data taken by the lambda-mode then were proceed by using linear un-mixing tool available in ZEN 2011 software package (Zeiss GmbH). All image processing was performed by using the same software. False colour images were adjusted to better distinguish the complexes from cellular organelles, *e.g.* yellow corresponds to complex, blue to DAPI that stains nucleus, green to nucleoli, and red to F-actin.

3. Results and discussion

3.1 Synthesis and single-crystal X-Ray determination

The investigated complexes, namely **Tol-Pt-4OHpy** and **CF_3-Pt-4OHpy** and the corresponding synthetic pathway for the preparation of ligands and complexes are shown in Chart 1 and Scheme S1 of the Electronic Supplementary Information (ESI), respectively. The 2,6-*bis*(3-(*p*-tolyl)-1*H*-1,2,4-triazol-5-yl)pyridine, namely **py-Tol-trzH_2**, tridentate 1igand was prepared in accordance with our already reported synthetic procedure.[42] The corresponding ligand bearing the trifluoro-methyl substituent on the triazole rings, 2,6-*bis*(3-(trifluoromethyl)-1*H*-1,2,4-triazol-5-yl)pyridine, namely **py-CF_3-trzH_2**, has been prepared in modest yields by following an already reported method with some modifications (see Experimental Section).[38,47]

The final complexes were prepared by using the synthetic procedure sketched in Scheme S1 of the ESI. The reaction consists of a one-pot synthesis which employs either **py-Tol-trzH_2** or **py-CF_3-trzH_2**, as the tridentate ligand, $PtCl_2(DMSO)_2$ (DMSO = dimethylsulfoxide) as the Pt(II) precursor, triethylamine as the base and 4-hydroxypyridine as the ancillary ligand in a 3:1 mixture of 2-methoxyethanol and water as the solvent. The reaction mixture was overnight heated at 83°C resulting in the formation of a highly emitting plentiful precipitate. The desired complexes were obtained by purification on column chromatography as highly emitting yellow powder and characterized by NMR and high-resolution mass spectrometry. Further synthetic details can be found in the Experimental Section.

The 4-hydroxypyridine has been chosen as the ancillary ligand to provide an amphiphilic character to the complexes while keeping the overall charge neutral nature of the compounds. Neutral square-planar platinum complexes are indeed expected to show higher aggregation tendency than charged counterparts, due to the fact that the latters might experience much higher repulsive electrostatic interactions when spatially near.

Single crystals of the platinum complex bearing the trifluoro-methyl moieties suitable for X-ray diffractometric

analysis were obtained by crystallization in DMSO at room temperature. The corresponding ORTEP diagram for the complex **CF_3-Pt-4OHpy**·2DMSO is displayed in Fig. 1. The crystal data and structural refinement parameters are listed in Table S1 of the ESI. In the crystal state, the complex adopts a square-planar arrangement around the platinum atom, distorted in order to comply with the geometrical constrains imposed by the formally-dianionic tridentate ligand. As far as the geometrical parameters are concerned, the N(py)–Pt [where py is pyridine] bond lengths are 1.995(16) and 2.029(16) Å for N(1)–Pt and N(8)–Pt, respectively, and the N(trz)–Pt [where trz is triazolate] distances are 2.014(10) and 2.024(10) Å for N(2)–Pt and N(5)–Pt, respectively. Also, the N(py)–Pt–N(trz) bond angles, namely N(1)–Pt–N(2) and N(1)–Pt–N(5), are 81.1(6)º and 79.3(6)º, respectively. These values are sizeably narrower than those one could expect for ideal chelating arrangement for square planar complexes (90°). Finally, the complex shows an close-to-planarity arrangement as demonstrated by the value of 3.1(10)º of the N(1)–Pt–N(8) out-of-plane bending angle adopted by the nitrogen atom, N(8), of the monodentate ancillary pyridine. All these crystallographic findings are in agreement with the already reported structures of Pt(II) complexes containing 1,2,4-triazolate ligands with a κN^1 coordination mode.[48-50] Noteworthy, in the crystal packing the complex molecules are organized in a parallel head-to-head staggered fashion, but no closed-shell Pt···Pt interaction (Pt···Pt distance = 4.845 Å) has been observed, resulting in a negligible interaction between neighbour molecules. Such absence of interaction could most likely be due to the presence of the DMSO molecules within the crystal structure engaged in hydrogen bond interaction with the OH moiety of the ancillary pyridine [O(1)–H(1)···O(2) = 1.66 Å and O(1)···O(2) = 2.50(2) Å].

3.2 Photophysical properties

The absorption spectra of both complexes in DMSO solution are shown in Fig. S5 of the ESI and the most meaningful photophysical data are summarized in Table 1.

The compounds display broad and featureless weak bands ($\varepsilon = 3.4 \times 10^3$ M^{-1} cm^{-1} and 2.2×10^3 M^{-1} cm^{-1} for **CF_3-Pt-4OHpy** and **Tol-Pt-4OHpy**, respectively) centred at around 390 nm, which can be attributed to spin-allowed metal-to-ligand charge-transfer (^{1}MLCT) transitions, as already reported for closely related complexes.[22,42,48] Interestingly, the intensity of the bands is very different even though the maxima are the same for both complexes. These bands are attributed to transitions that mainly involve the platinum d orbitals partially mixed with the terdentate-ligand-centered π and π^* orbitals. Complex **Tol-Pt-4OHpy** presents a strong featureless band at about 320 nm attributed to ligand-centered (^{1}LC) $\pi \rightarrow \pi^*$ transitions involving the tolyl groups on the triazolate rings. At higher energies, triazoles and pyridine bands overlap and it is not possible to assign the correct maxima within the window of the employed solvent.

Excitation at any of the absorption bands causes an emission at room temperature in DMSO only for the **Tol-Pt-4OHpy** (Fig. 2), with a maximum at 534 nm, while the trifluoro-methyl derivative is not emissive in fluid solution. The excitation spectrum is also depicted in Fig. 2 and it is very similar to the absorption spectrum recorded in the same conditions (Fig. S5 of the ESI). Interestingly, addition of water in the DMSO solution, DMSO:H_2O (1:99 $^v/_v$), causes the formation of aggregates for both the tolyl- and the CF_3-containing derivatives. For the **Tol-Pt-4OHpy** the emission shifts to lower energy (Fig. 2) reaching a maximum at 562 nm, while the **CF_3-Pt-4OHpy** displays now an emission at 587 nm. The fact that aggregates are formed is also visible looking at the excitation spectra as clearly demonstrated by the formation of a new broad band around 450 nm for the tolyl complex while for the **CF_3-Pt-4OHpy** derivative the onset shifts to very low energy reaching 520 nm (Fig. 2). These low energy bands, which are absent in the pure DMSO solutions, are attributed to the transitions involving a new excited state, namely ^{3}MMLCT, which is promoted by metallophilic interactions between platinum centers. The emission of the complex **CF_3-Pt-4OHpy**, as monomeric species, can be detected at 77 K in 2-MeTHF glassy matrix. The structured emission presents vibrational sharp peaks at 452, 482 and 515 nm, and it is attributed mainly to ligand centred (LC) transitions in accordance with a similar previously reported complex (Fig. 2).[38]

At room temperature, the excited state lifetimes of the complexes show multi-exponential kinetics and, for **Tol-Pt-4OHpy**, they become longer going from pure DMSO to DMSO/H_2O condition. This behaviour mirrors the fact that we are most likely in the presence of aggregates as well as that both monomers and assemblies of different size are present and emissive. We believe that the longest component, being 1772 ns (19%) and 365 ns (14%) for **Tol-Pt-4OHpy** and **CF_3-Pt-4OHpy**, respectively, is always associated to the most packed aggregates which prevent dioxygen diffusion reducing emission quenching. Noteworthy, the emission quantum yield for **CF_3-Pt-4OHpy** reaches a value as high as 36% in the aggregate form in air-equilibrated DMSO:H_2O (1:99 $^v/_v$) condition.

3.3 Bio-imaging

Due to the dynamic behaviour between monomeric and aggregates species, monitored following the changes in the photophysical properties, we have investigated the possible use of the complexes as probes for optical imaging in living and fixed cells.

The two complexes possess terdentate ligands with different hydrophobicity and electron density. Furthermore, **CF_3-Pt-4OHpy** has been chosen because trifluoromethyl groups are known to enhance cell and nuclear permeability, while lipophilicity generally enhance cellular uptake even though being responsible of increased cytotoxicity.[51-52] On the other hand, **Tol-Pt-4OHpy** derivative displays good luminescent properties in both monomeric and aggregated conditions.

The platinum complexes were dissolved in a minimum amount of DMSO and the respective solutions were diluted into phosphate buffer saline, PBS, resulting in a 50 μM solution with less than 1% content in DMSO. HeLa cells were incubated for 4 hours at 37° C under 5% CO_2 atmosphere with the complexes, and then were washed with complex-free PBS, followed by cell fixation using 4% paraformaldehyde (PFA) solution. In addition, kinetic experiments to observe the real time internalization of the complex were performed (data not shown).

As shown in the confocal microscopy images, Fig. 3a and Fig. 4a, the two complexes show bright emission coming from different cellular compartments indicating cell internalization.[22] The emission of **Tol-Pt-4OHpy** was mainly observed from cytoplasmic region while the trifluoromethyl-containing complex, *i.e.* **CF_3-Pt-4OHpy**, was partially distributed in the cytoplasmic region but bright aggregates were observed inside the nucleus. At this stage we have no evidence if the metal complexes are internalized as monomeric species and then aggregate inside cells or they are uptaken as small aggregates. The emission spectra taken from the highly emissive spots clearly demonstrate that for both complexes the emission energy and shape correspond to those of the assembled systems in DMSO/water solution (see Fig. 3b and 4b). To have a better understanding of the localization of the **CF_3-Pt-4OHpy** complex, co-localization studies were performed by staining the three regions where we observe the orange emission. The cells were labelled with 4',6-diamidino-2-phenylindole-6-carboxamidine (DAPI) (nucleus label), Phalloidin Alexa Fluor® 568 (F-actin stain) and SYTO® RNASelect™ Green Fluorescent Cell Stain (nucleoli stain). As depicted in Fig. 5a-b, **CF_3-Pt-4OHpy** is able to localize into cytoplasm and also inside the nucleus. The perfect overlap of the emission of the complex and the SYTO® RNASelect™ green fluorescence indicates that the assemblies are present in the nucleoli (Fig. 5b). To prove that the complex is really inside the cell we have also done *z*-scan acquisitions by means of a confocal microscope and the results are displayed Fig. 5c.

Interestingly, these complexes showing aggregation process through (extended) ground-state $d_z2\cdots d_z2$ metallophilic interactions possess low-lying ^{1}MMLCT state. As can be clearly seen from Fig. 2 we should be able to excite the systems also in the visible region since the excitation spectrum extend to almost 550 nm. To prove that excitation can be as low as 543 nm, we have recorded emission images upon different excitation wavelengths and showed that we can efficiently use this complex and overcome the problem related to the excitation energy as shown for **CF_3-Pt-4OHpy** in Fig. S6 of the ESI. The aggregation process is also leading to the protection of the platinum complexes and prevents oxygen quenching, as already discussed above, but also to reduced photobleaching. In order to estimate to a certain extent the degree of photostability of the investigated systems inside nucleus of cells, we have compared the photobleaching time of DAPI, used to stain nuclear region, with our platinum complexes upon excitation at the same wavelength, 405 nm. The results are displayed in Fig. S7 and clearly suggest that our label is more photostable than the organic dye.

We wish to point out that the uptake of the platinum complexes and their internalization in HeLa cells occur only when PBS is used as culture media. Indeed, the replacement of PBS with cell culture media prevented the complexes to be internalized by the cells. Fig. S8 shows the experiments carried out for the complex **CF_3-Pt-4OHpy**. The data obtained suggest that the platinum complex is somehow sequestered by the culture media, most likely because of an interaction with one of the proteins, and therefore is not uptaken by the cells even if the incubation time is extended to 24 hours. Furthermore, to confirm this hypothesis, the complex was incubated for 20 minutes in PBS solution with cells and, as expected, internalization occurred (Fig. 6a). At this point, the cells were washed several times with PBS to eliminate the excess of the complex and the PBS was replaced by normal culture media. After several minutes (see Movie S1 and Fig. 6b-c), the luminescence slowly disappears from inside the cells and surprisingly it has been detected in bright small spots surrounding the cells, but clearly in the cell culture media. In addition, the emission profile collected from several of these aggregates confirms that photoluminescence is coming from the platinum compounds, but the wavelengths (λ_{em} = 550 nm) is hypsochromically shifted compared with the platinum aggregates inside the cells. This observation supports the hypothesis that the platinum complexes experience a different environment and therefore change their emission properties.

However, internalization of the platinum complexes using cell culture media as the incubating media can occur if the cells are dying or cell membrane is partly damaged. Live cell imaging was performed on HeLa cells incubated with **CF_3-Pt-4OHpy** in cell culture media using time-lapse acquisition mode. The complex was excited at 405 nm and the emission signal was collected with one-minute acquisition time for a total duration of 75 minutes. The slices of time-lapse images for 0 to 75 minutes can be seen in Fig. 7 (see also Movie S2 of the ESI). Our findings reveal that there was no uptake occurring before the first 30 minutes, but surprisingly the uptake of the complex starts very rapidly only when the cells were dying due to the long exposure to UV light (see formation of apoptotic sign in Movie S2, bright field image, after one hour). This is indeed not surprising since, as already reported, long exposure to UV light can harm the cell, break cell membrane, damage DNA and other cellular organelles and later induce cell death.[53] In fact, this specific uptake phenomenon has been observed and well studied especially in the development of dead cell labelling molecules.

As shown Fig. 7 d-e, this finding is also strongly supported by the fact that only area irradiated with UV light show cellular uptake of the complex while cells in the surrounding do not exhibit any internalization since they have not been damaged. A control experiment to prove that the platinum complex is not responsible for the cell damage due to the formation of singlet oxygen or other reactive species was performed by irradiating

the system, in the same conditions, with wavelengths of 455 and 488 nm light where the platinum complexes absorb light.

4. Conclusion

We have demonstrated the use of metal complexes and in particular of luminescent Pt(II) systems for bioimaging. Their square planar geometry can induce self-assembly resulting in supramolecular architectures possessing interesting photophysical properties together with an enhanced stability. Such aggregates can be indeed considered a new class of dynamic probes, since the emission can be easily modulated and their long-lived emission easily detected. Also by designing the coordinating ligands it is possible to internalize and localize the complexes in specific parts of the cells.

The investigated complexes show efficient uptake when specific incubation conditions *e.g.* PBS was used and, interestingly, the presence of proteins or other biomolecules can inhibit or even sequester the platinum complexes forcing expulsion from cells after their internalization. Irradiation of the cells with 405 nm light causes fast uptake of the compounds due to cell damage.

5. Acknowledgements

The authors kindly acknowledge University of Strasbourg, CNRS and ERC grant n. 2009-247365 for financial support. L.D.C. is grateful to the Région Alsace and the Communauté Urbaine de Strasbourg for the award of a Gutenberg Excellence Chair (2011-2012) and to AXA Research funds. The authors gratefully acknowledge the International Center for Frontier Research in Chemistry (icFRC), the Région Alsace, the Communauté Urbaine de Strasbourg, the Département du Bas-Rhin, and the LabEx Chimie des Systèmes Complexes for funding the purchase of the Zeiss LSM 710 confocal microscope. The authors kindly acknowledge Dr. C. Bailly and Dr. L. Brelot, University of Strasbourg, for single crystal X-ray diffractometric determination.

Notes and references

[a] ISIS & icFRC, Université de Strasbourg & CNRS, 8 rue Gaspard Monge, 67000 Strasbourg, France. E-mail: mauro@unistra.fr, decola@unistra.fr; Fax: +33 (0) 3 6885 5242; Tel: +33 (0) 3 6885 5220
[b] University of Strasbourg Institute for Advanced Study (USIAS), 5 allée du Général Rouvillois, 67083 Strasbourg, France.

† Electronic Supplementary Information (ESI) available: synthetic scheme, photophysical, bio-imaging and crystallographic data can be found as supplementary information. CCDC-988918 contains the crystallographic data for **CF_3-Pt-4OHpy**·2DMSO complex. These data can be obtained free of charge from the Cambridge Crystallographic Data Centre. See DOI: 10.1039/b000000x/

1 N. Darmawan, C.-H. Yang, M. Mauro, M. Raynal, S. Heun, J. Pan, H. Buchholz, P. Braunstein, L. De Cola, *Inorg. Chem.*, 2013, **52**, 10756–10765.
2 M. S. Lowry, S. Bernhard, *Chem. Eur. J.*, 2006, **12**, 7970–7977; Y. You, S. Y. Park, *Dalton Trans.*, 2009, 1267–1282.
3 Y. Kawamura, K. Goushi, J. Brooks, J. J. Brown, H. Sasabe, C. Adachi, *App. Phys. Lett.*, 2005, **86**, 071104–071107.
4 X.-C. Hang, T. Fleetham, E. Turner, J. Brooks, J. Li, *Angew. Chem. Int. Ed.*, **2013**, *52*, 6753–6756.
5 H. Yersin (Ed.) *Highly Efficient OLEDs with Phosphorescent Materials*, Wiley-VCH, Weinheim, Germany, 2008
6 M. E. Thompson, P. E. Djurovich, S. Barlow and S. Marder, *Organometallic Complexes for Optoelectronic Application*s, in *Comprehensive Organometallic Chemistry III*, ed. R. H. Crabtree and D. M. P. Mingos, Elsevier, Oxford, UK, 2006.
7 H. Xu, R. Chen, Q. Sun, W. Lai, Q. Su, W. Huang, X. Liu, *Chem. Soc. Rev.*, **43**, 3259-3302, 2014.
8 R. D. Costa, E. Ortí, H. J. Bolink, F. Monti, G. Accorsi, N. Armaroli, *Angew. Chem. Int. Ed.*, 2012, **51**, 8178–8211.
9 T. Hu, L. He, L. Duan, Y. Qiu, *J. Mater. Chem.*, 2012, **22**, 4206–4215.
10 S. C. F. Kui, F.-F. Hung, S.-L. Lai, M.-Y Yuen, C.-C. Kwok, K.-H. Low, S. S.-Y. Chui, C.-M. Che, *Chem. Eur. J.*, 2012, **18**, 96–109.
11 P.-T. Chou, Y. Chi, *Chem. Eur. J.,* 2007, **13**, 380-395; Y. You, S. Y. Park, *Dalton Trans.*, 2009, 1267–1282.
12 M. Panigati, M. Mauro, D. Donghi, P. Mercandelli, P. Mussini, L. De Cola, G. D'Alfonso, *Coord. Chem. Rev.*, 2012, **256**, 1621–1643.
13 Y. Yang, Q. Zhao, W. Feng, F. Li, *Chem. Rev.*, 2013, **113**, 192–270.
14 X. Chen, T. Pradhan, F. Wang, J. S. Kim, J. Yoon, *Chem. Rev.*, 2012, **112**, 1910–1956.
15 C. Y.-S. Chung, K. H.-Y. Chan, V. W.-W. Yam, *Chem. Commun.*, 2011, **47**, 2000–2002.
16 P. Wu, E. L.-M. Wong, D.-L. Ma, G. S.-M. Tong, K.-M. Ng, C.-M. Che, *Chem. Eur. J.*, 2009, **15**, 3652–3656.
17 A. Ruggi, F. W. B. van Leeuwen, A. H. Velders, *Coord. Chem. Rev.*, 2011, **255**, 2542–2554.
18 V. Fernández-Moreira, F. L. Thorp-Greenwood, M. P. Coogan, *Chem. Commun.*, 2010, **46**, 186–202.
19 E. Baggaley, J. A. Weinstein, J. A. G. Williams, *Coord. Chem. Rev.*, 2012, **256**, 1762–1785.
20 Q. Zhao, C. Huang, F. Li, *Chem. Soc. Rev.*, 2011, **40**, 2508–2524.
21 K. K.-W. Lo, A. W.-T. Choi, W. H.-T. Law, *Dalton Trans.*, 2012 **41**, 6021–6047.
22 M. Mauro, A. Aliprandi, D. Septiadi, N. S. Kehr, L. De Cola, *Chem. Soc. Rev.*, **2014**, doi: 10.1039/C3CS60453E.
23 R. Y. Tsien, *Angew. Chem. Int. Ed.*, 2009, **48**, 5612–5626.
24 R. D. Moriarty, A. Martin, K. Adamson, E. O'Reilly, P. Mollard, R. J. Forster, T. E. Keyes, *J. Microscopy*, 2014, **253**, 204–218.
25 Z. Guo, S. Park, J. Yoon, I. Shin, *Chem. Soc. Rev.*, 2014, **43**, 16–29.
26 H. Andersson, T. Baechi, M. Hoechl, C. Richter, *J. Microscopy*, 1998, **191**, 1–7.
27 J. E. Aubin, *J. Histochem. Cytochem.*, 1979, **27**, 36–43.
28 S. W. Botchway, M. Charnley, J. W. Haycock, A. W. Parker, D. L. Rochester, J. A. Weinstein, J. A. G. Williams, *Proc. Nat. Acad. Sci. USA*, 2008, **105**, 16071–16076.
29 V. Balzani, G. Bergamini, P. Ceroni, *Adv. Inorg. Chem.*, 2011, **63**, 105–135.
30 V. Balzani, G. Bergamini, P. Ceroni, F. Vögtle, *Coord. Chem. Rev.*, 2007, **251**, 525–535.

31 T. Qin, J. Ding, L. Wang, M. Baumgarten, G. Zhou, K. Müllen, *J. Am. Chem. Soc.*, 2009, **131**, 14329–14336.
32 S.-C. Lo, G. J. Richards, P. J. J. Markham, E. B. Namdas, S. Sharma, P. L. Burn, D. W. I. Samuel, *Adv. Funct. Mater.*, 2005, **15**, 1451–1458.
33 M. Mauro, G. De Paoli, M. Otter, D. Donghi, G. D'Alfonso, L. De Cola, *Dalton Trans.*, 2011, **40**, 12106–12116.
34 E. Baggaley, S. W. Botchway, J. W. Haycock, H. Morris, I. V. Sazanovich, J. A. G. Williams, J. A. Weinstein, *Chem. Sci.*, 2014, **5**, 879–886.
35 J. M. Baumes, J. J. Gassensmith, J. Giblin, J.-J. Lee, A. G. White, W. J. Culligan, W. M. Leevy, M. Kuno, B. D. Smith, *Nat. Chem.*, 2010, **2**, 1025–1030.
36 J. O. Escobedo, O. Rusin, S. Lim, R. M. Strongin, *Curr. Opin. Chem. Bio.*, 2010, **14**, 64–70.
37 S. A. Hilderbrand, R. Weissleder, *Curr. Opin. Chem. Bio.*, 2010, **14**, 71–79.
38 M. Mauro, A. Aliprandi, C. Cebrián, D. Wang, C. Kübel, L. De Cola, *Chem. Commun.*, 2014, doi:10.1039/c4cc01045k.
39 C. A. Strassert, C.-H. Chien, M. D. Galvez Lopez, D. Kourkoulos, D. Hertel, K. Meerholz, L. De Cola, *Angew. Chem. Int. Ed.*, 2011, **50**, 946–950.
40 N. Komiya, N. Itami, T. Naota, *Chem. Eur. J.*, 2013, **19**, 9497–9505.
41 R. Romeo, L. M. Scolaro, *Inorg. Synth.,* 1998, **32**, 149–153.
42 M. Mydlak, M. Mauro, F. Polo, M. Felicetti, J. Leonhardt, G. Diener, L. De Cola, C. A. Strassert, *Chem. Mater.*, 2011, **23**, 3659–3667.
43 Kappa CCD Operation Manual, Nonius B. V., Ed.; Delft: The Netherlands, 1997.
44 G. M. Sheldrick, *Acta Crystallogr.,* 1990, **A46**, 467–473.
45 G. Sheldrick, SHELXL-97, Universität Göttingen, Göttingen, Germany, 1999.
46 A. L. Spek, *J. Appl. Cryst.*, 2003, **36**, 7–13.
47 K. Funabiki, N. Noma, G. Kuzuya, M. Matsui, K. Shibata, *J. Chem. Res. (S)*, 1999, 300–301.
48 C. Cebrián, M. Mauro, D. Kourkoulos, P. Mercandelli, D. Hertel, K. Meerholz, C. A. Strassert, L. De Cola, *Adv. Mater.*, 2013, **25**, 437–442.
49 A. I. Matesanz , P. Souza , *J. Inorg. Biochem.* 2007, **101**, 245–253.
50 H.-Y. Hsieh , C.-H. Lin , G.-M Tu , Y. Chi , G.-H. Lee, *Inorg. Chim. Acta*, 2009, **362**, 4734–4739.
51 H. L. Yale, J. *Med. Chem*., 1958, **1**, 121–133;
52 S. Purser, P. R. Moore, S. Swallow, V. Gouverneur, *Chem. Soc. Rev*., 2008, **37**, 320–330.
53 K. V. Bogdanov, A. B. Chukhlovin, A. Y. Zaritskey, O. I. Frolova, B. V. Afanasiev, *Brit. J. Haematology*, 1997, **98**, 869-872.

Journal Name RSCPublishing

ARTICLE

Figures and Tables

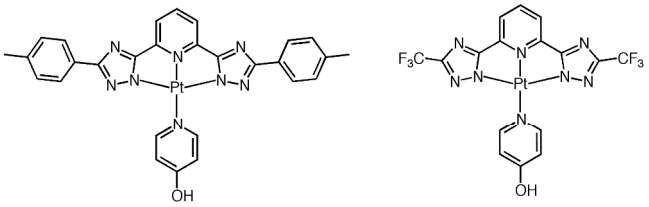

Chart 1. Chemical formulas and abbreviations of the platinum complexes investigated.

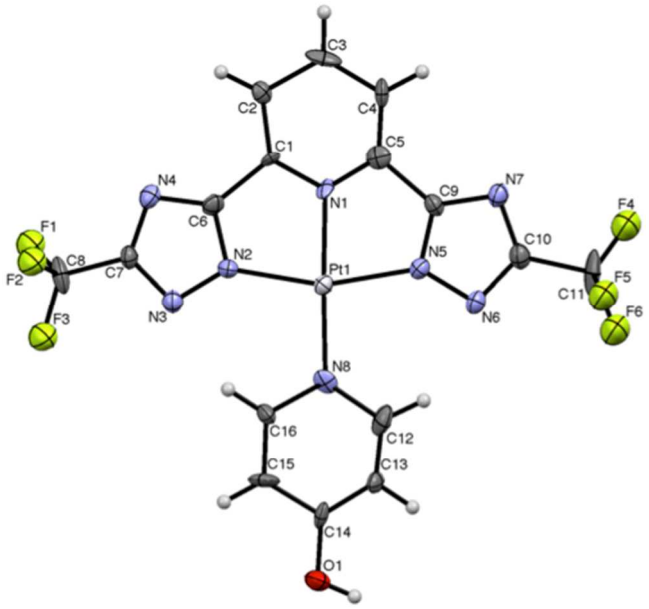

Fig. 1. ORTEP diagram of complex **CF_3-Pt-4OHpy**·2DMSO with thermal ellipsoids shown at 30% probability level with corresponding atom labelling. The two DMSO solvent molecules are omitted for sake of clarity. Selected bond lengths (Å) and angles (º): N(1)–Pt = 1.995(16), N(2)–Pt = 2.014, N(5)–Pt = 2.024(10), N(8)–Pt = 2.029(16), N(1)–Pt–N(2) = 81.1(6), N(1)–Pt–N(5) = 79.3(6), N(2)–Pt–N(8) = 101.0(6), N(5)–Pt–N(8) 98.5(6).

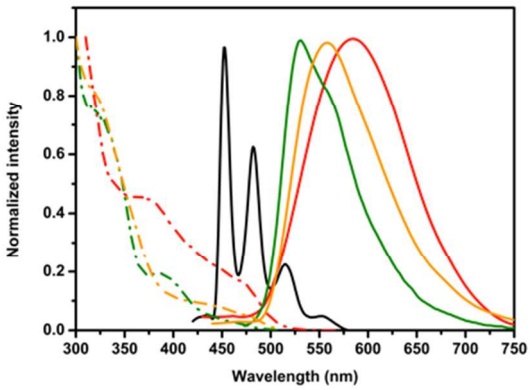

Fig. 2. Emission (solid traces) and excitation (— · —) spectra for complexes **Tol-Pt-4OHpy** and **CF_3-Pt-4OHpy** in different conditions. Emission and excitation for **Tol-Pt-4OHpy** in pure DMSO (green traces) and in DMSO:H_2O (1:99 $^v/_v$) (orange trace); **CF_3-Pt-4OHpy** at 77 K in 2-MeTHF glassy matrix (black trace) and in DMSO:H_2O (1:99 $^v/_v$) (red trace). The samples were excited at λ_{exc} = 330 nm.

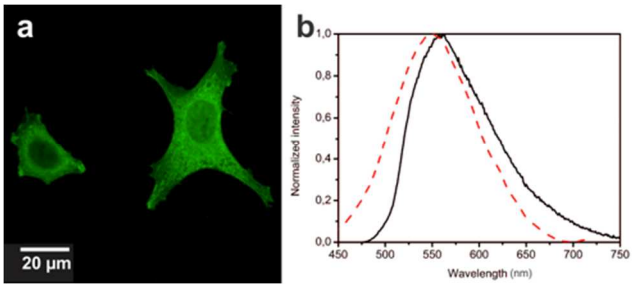

Fig. 3. (a) Luminescence confocal microscopy images showing the distribution of complex **Tol-Pt-4OHpy** inside HeLa cells; (b) Emission spectra recorded for DMSO:H_2O condition (solid black trace) and collected from the cytoplasmic region of the cells (dashed red trace). The samples were excited at λ_{exc} = 330 and 405 nm for solvents and cell experiments, respectively.

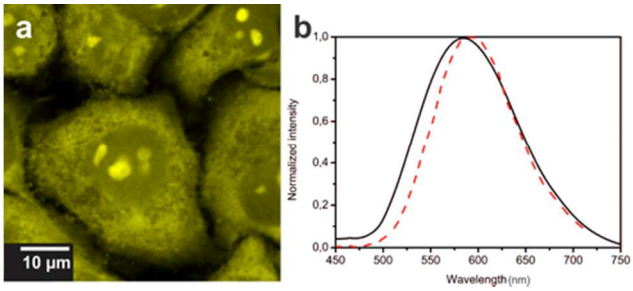

Fig. 4. (a) Luminescence confocal microscopy images showing the distribution of **CF_3-Pt-4OHpy** inside HeLa cells; (b) Emission spectra recorded in DMSO:H_2O solution (black solid trace) and from the bright aggregate inside the nuclear region (dashed red trace). The samples were excited at λ_{exc} = 330 and 405 nm for solvents and cell experiments, respectively.

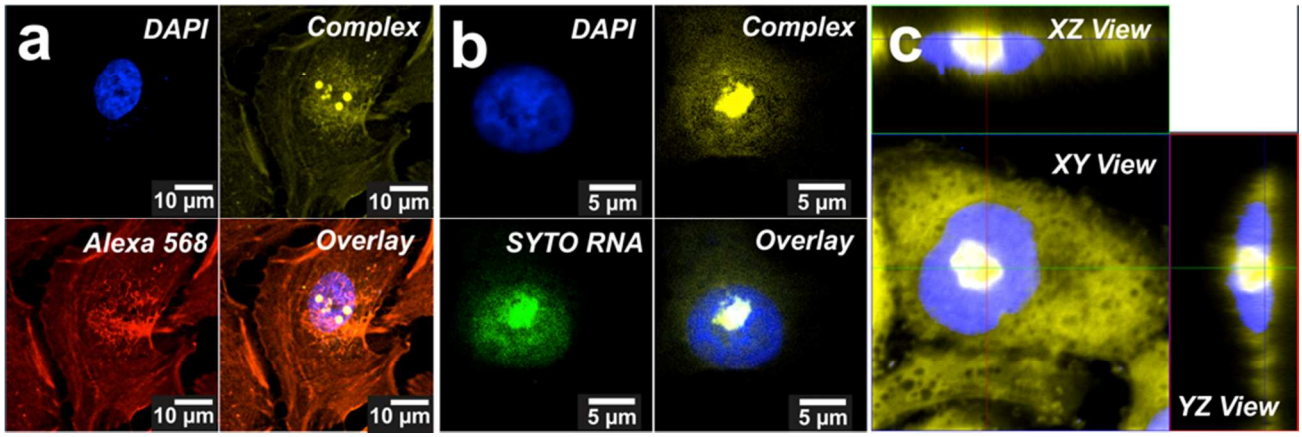

Fig. 5. Confocal microscopy images of the distribution of **CF_3-Pt-4OHpy** inside HeLa cells. (a) DAPI staining of nucleus, complex **CF_3-Pt-4OHpy**, Phalloidin Alexa Fluor® 568 stains F-actin inside cytoplasmic region, overlay of three images. The excitation wavelength for DAPI and **CF_3-Pt-4OHpy** was 405 nm, while Phalloidin Alexa Fluor® 568 was excited at 594 nm. Localization experiments (b) showing DAPI staining the nucleus, SYTO® RNASelect™ Green Fluorescent Cell Stain labelling the nucleoli (λ_{exc} = 488 nm), and in yellow the emission of **CF_3-Pt-4OHpy**. The overlay image suggests that the aggregates are confined in the nucleoli. (c) Orthogonal view of the image showing a very bright signal (yellow) due to **CF_3-Pt-4OHpy** aggregates coming from inside the nuclear region and co-localized into the nucleoli. Blue color is due to the DAPI staining.

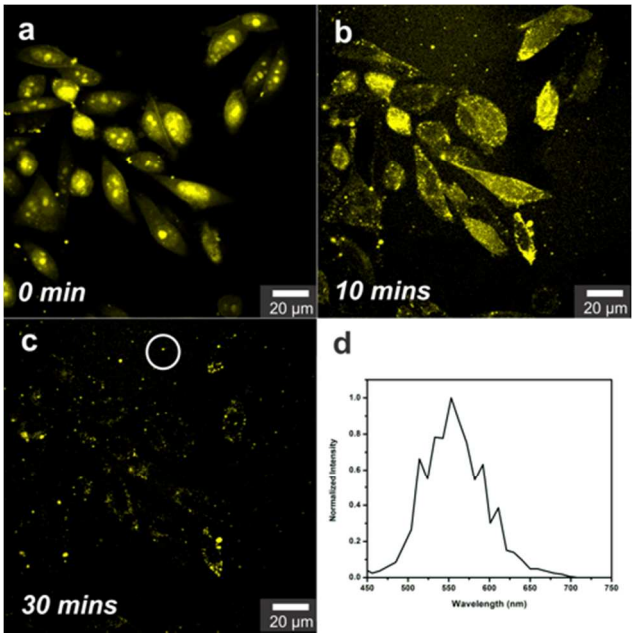

Fig. 6 The complex **CF_3-Pt-4OHpy** is aggregated inside the nucleus after 20 min incubation in PBS and replacement of the PBS with cell culture media causes its externalization in few minutes: (a) 0 minute, (b) 10 minutes, and (c) 30 minutes. (d) Emission spectrum recorded from the small aggregates in the white circle region, showing a maximum centred at 550 nm.

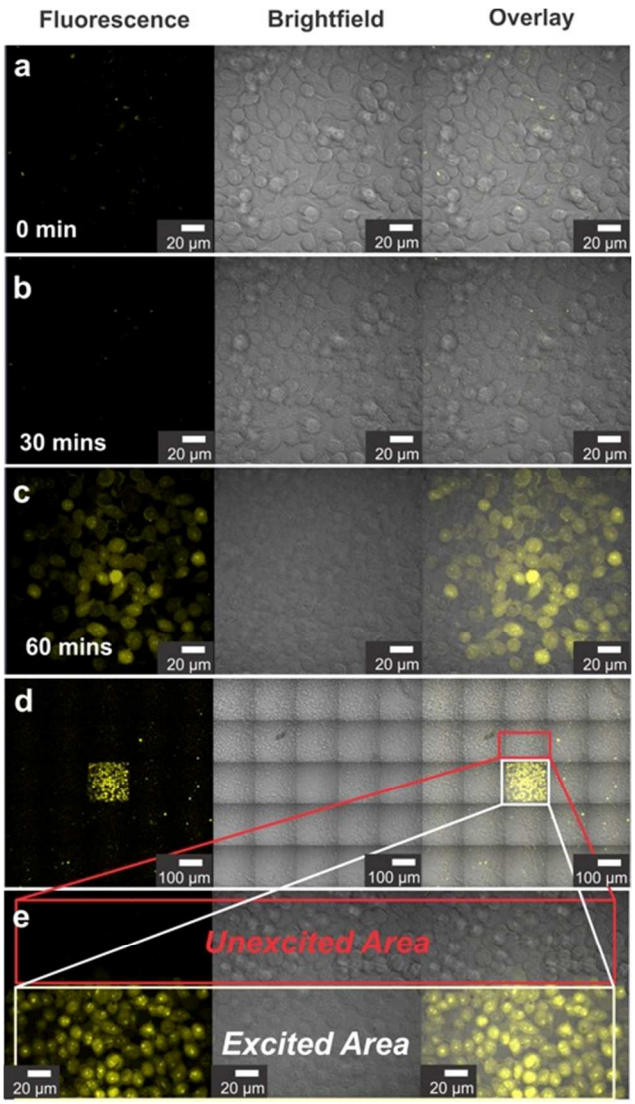

Fig. 7. Time-lapse images showing the light-induced internalization of **CF_3-Pt-4OHpy** in culture media after different irradiation times: (a) 0 minute, (b) 30 minutes, and (c) 60 minutes. (d) zoom-out view; (e) zoom-in view showing the unexcited region and the area exposed to the 405 nm laser irradiation.

Table 1. Most meaningful photophysical data for complexes **Tol-Pt-4OHpy** and **CF_3-Pt-4OHpy** in DMSO and DMSO:H_2O (1:99 $^v/_v$) conditions.

Compound					DMSO:H_2O 1:99		
	λ_{abs} (ε) [nm, $\times10^3$ M^{-1} cm^{-1}]	λ_{em} [nm]	τ [ns]	PLQY (%)	λ_{em} [nm]	τ [ns]	PLQY (%)
CF_3-Pt-4OHpy	392 (3.4)[a]	452, 482, 515[b]	–	–	587	163 (57%) 22 (28%) 365 (14%)	36
Tol-Pt-4OHpy	322 (14.9), 390 (2.0)[a]	534[a]	5.1 (26%) 205 (67%) 476 (7%)	1.2[a]	562	662 (55%) 139 (27%) 1772 (19%)	2.8

[a] measured in DMSO at room temperature; [b] measured at 77 K in 2Me-THF glassy matrix.